Amyloid β induces cardiac dysfunction and neuro-signaling impairment in the heart of an Alzheimer's disease model.

Andrea Elia[1], Rebecca Parodi-Rullan[1], Rafael Vazquez-Torres[1], Ashley Carey[1], Sabzali Javadov[2], and Silvia Fossati[1].

[1]Alzheimer's Center at Temple (ACT), Department of Neural Sciences, Lewis Katz School of Medicine, Temple University, 3500 N Broad St, Philadelphia, PA 19140.

[2] Department of Physiology, University of Puerto Rico School of Medicine, San Juan, PR 00936-5067, USA

Corresponding author: Silvia Fossati; silvia.fossati@temple.edu

Short Title: *Cardiac amyloidosis in the Tg2576 model of AD.*

Abstract

Aims: Alzheimer's disease (AD) is a complex neurodegenerative disorder characterized by cerebral amyloid β (Aβ) deposition and tau pathology. The AD-mediated degeneration of the brain neuro-signaling pathways, together with a potential peripheral amyloid accumulation, may also result in the derangement of the peripheral nervous system, culminating in detrimental effects on other organs, including the heart. However, whether and how AD pathology modulates cardiac function, neurotrophins, innervation, and amyloidosis is still unknown. Here, we report for the first time that cardiac remodeling, amyloid deposition, and neuro-signaling dysregulation occur in the heart of Tg2576 mice, a widely used model of AD and cerebral amyloidosis. **Methods ad Results:** Echocardiographic analysis showed significant deterioration of left ventricle function, evidenced by a decline of both ejection fraction and fraction shortening percentage in 12-month-old Tg2576 mice compared to age-matched WT littermates. Tg2576 mice hearts exhibited an accumulation of amyloid aggregates, including Aβ, an increase in interstitial fibrosis and severe cardiac nervous system dysfunction. The transgenic mice also showed a significant decrease in cardiac nerve fiber density, including both adrenergic and regenerating nerve endings. This myocardial denervation was accompanied by a robust reduction in NGF and BDNF protein expression as well as GAP-43 expression (regenerating fibers) in both the brain and heart of Tg2576 mice. Accordingly, cardiomyocytes and neuronal cells challenged with Aβ oligomers showed significant downregulation of BDNF and GAP-43, indicating a causal effect of Aβ on the loss of cardiac neurotrophic function. **Conclusions:** Overall, this study uncovers possible harmful effects of AD on the heart, revealing cardiac degeneration induced by Aβ through fibrosis and neuro-signaling pathway deregulation for the first time in Tg2576 mice. Our data suggest that AD pathology can cause deleterious effects on the heart, and the peripheral neurotrophic pathway may represent a potential therapeutic target to limit these effects.

Keywords: Amyloid-β (Aβ), Alzheimer’s disease, cardiac dysfunction, neurotrophic pathway, peripheral nervous system, brain-heart axis

1. Introduction

Alzheimer's disease (AD) is the most common form of dementia, with a significantly growing incidence that is expected to triple by 2050, especially due to the increasing population age in developed countries[1]. This complex neurodegenerative disorder is characterized by the progressive accumulation of insoluble amyloid-β (Aβ) plaques in the brain parenchyma and vasculature, together with neurofibrillary tangles of hyperphosphorylated tau, resulting in a widespread cerebral derangement[2]. This culminates in severe neuronal loss, neuroinflammation, and vascular dysfunction with increased blood-brain barrier (BBB) permeability and progressive cognitive decline[3-5]. Albeit the main symptoms of the disease predominantly concern the central nervous system (CNS), recent evidence described extracerebral effects of AD that involve the heart, among other peripherical organs and tissues[6]. Indeed, several studies have demonstrated a connection between AD and cardiac disorders[7-9]. Particularly, beyond the neuronal areas, Aβ accumulation was found in the cardiac tissue of AD patients[10] similar to that detected in patients with idiopathic dilated cardiomyopathy[11, 12]. In parallel to the described neuronal and vascular dysfunction, AD is accompanied by a dysregulation in the brain neurotrophic signaling, with a progressive loss of the two main neuromodulators, nerve growth factor (NGF) and brain-derived neurotrophic factor (BDNF)[13]. Specifically, Aβ significantly affects the expression of these neurotrophins, and the maladaptive remodeling of the neuro-signaling pathway is associated with cognitive decline[14]. Therefore, it is plausible to hypothesize that the progressive neurotrophic signaling degeneration observed in the brain of AD patients may trigger a gradual decline in peripheral levels of neuromodulators. The latter, in turn, may result in a severe derangement of other peripheral organs, including the cardiac nervous system, potentially culminating in lethal heart dysfunction. However, whether and how AD pathology modulates neurotrophic factors (NTFs) levels, innervation, and amyloidosis in the cardiac tissue remains to be explored. Previous studies have described the accumulation of both Aβ peptides, Aβ42 and Aβ40, in the myocardial parenchyma of AD patients[10], associated with progressive cardiac dysfunction, supporting the hypothesis that AD is a multi-organ disease. Yet, the mechanisms involved in cardiac dysfunction and peripheral autonomic nervous system derangement in AD remain elusive, and

77 whether Aβ aggregates reside outside the central nervous system colonizing the
78 myocardial parenchyma and fueling cardiac impairment is still under debate. Moreover,
79 early reports have attested to the detrimental effects mediated by Aβ oligomers on the
80 neurotrophic signaling pathway in the brain, with a progressive reduction in both
81 production and release of neurotrophins, associated with severe cerebral
82 degeneration[15, 16]. However, there are no studies about the potential impacts of AD
83 pathology on the modulation of peripheral nervous system activity and cardiac availability
84 of neurotrophins. Of note, it is known that a decline in circulating BDNF levels promotes
85 the progression of cardiac disease, especially that of ischemic etiology[17-19].
86 Nevertheless, to the best of our knowledge, no studies thus far analyzed whether AD
87 pathology and more specifically cerebral amyloidosis have an impact on cardiac
88 functional homeostasis. This study, moving on from clinical studies that show diastolic
89 dysfunction in AD patients, directly demonstrates the effect of Aβ pathology on cardiac
90 dysfunction mechanisms. Moreover, we investigated whether the accumulation of cardiac
91 Aβ aggregates is associated with alterations of peripheral innervation and neurotrophins,
92 such as BDNF and NGF, in the heart. Overall, we determined for the first time the
93 presence of cardiac functional impairments, cardiac parenchymal fibrosis and
94 amyloidosis, neurotrophic signaling pathway deficiency, and nerve fiber loss in the
95 Tg2576 mouse model of AD.

96 **2. Methods**

97 **2.1 Animals**

98 Male and female Tg2576 mice, a model of cerebral amyloidosis bearing the Swedish
99 mutation (KM670/671NL), and age-matched WT littermates were bred internally. Mice
100 were maintained under controlled conditions (~22°C, and in a 12-hour light-dark cycle,
101 lights on 7 am to 7 pm) with unrestricted access to food and water. The generation of
102 B6;SJL-Tg(APPSWE)2576Kha mice (Tg2576) on a B6;SJL Mixed Background was as
103 described[20].Tg-2576 mice develop numerous parenchymal amyloid beta plaques at 11-
104 13 months and cerebral amyloid angiopathy (CAA) at 10-11 months of age[21]. Tg2576
105 and age-matched WT littermates (males and females) were evaluated at 4- and 12-
106 month-old age. All experiments and animal protocols were performed according to

107 protocols approved by the Institutional Animal Care and Use Committee of Temple
108 University School of Medicine and conformed to the National Research Council Guide for
109 the Care and Use of Laboratory Animals published by the US National Institutes of Health
110 (2011, eighth edition).

111 **2.2. Assessment of cardiac function by transthoracic echocardiography**

112 Transthoracic bi-dimensional M-mode echocardiographic analysis was accomplished in
113 4 and 12 months-old mice under anesthesia, before and after the development of Aβ
114 pathology, using a VisualSonics Vevo 2100 system (VisualSonics, Toronto, Canada).
115 Cardiac function and structure were evaluated by measuring left ventricle (LV) wall
116 thickness, end-diastolic diameter (LVEDD), end-systolic diameter (LVESD), end-diastolic
117 volume (LVEDV), end-systolic volume (LVESV), ejection fraction (EF%), and fraction
118 shortening (FS%) percentage[22]. Animals were euthanized at 12 months for organ
119 explant and biomolecular and histological analysis.

120 **2.3 Tissue processing and morphological evaluations**

121 Cardiac specimens were fixed in Zamboni's solution (2% paraformaldehyde and picric
122 acid) overnight at 4°C, then cryoprotected with 20% sucrose in PBS for 24 hours at 4°C
123 and cut in 5-μm-consecutive thick longitudinal sections using a freezing sliding microtome
124 (Leica 2000R, Germany). Interstitial fibrosis was assessed via Picro Sirius Red Stain Kit
125 (Abcam, ab150681), and images were acquired using a Nikon Eclipse Ti fluorescence
126 microscope with an 20x objective[23]. Cardiac fibrosis density was measured using
127 ImageJ software (NIH, version 1.30) and expressed as a percentage of fibrotic area over
128 the total area. A single operator blindly executed all the quantifications.

129 **2.4 Immunostaining**

130 The cardiac sections were processed via the indirect immunofluorescence method using
131 rabbit polyclonal antibodies against tyrosine hydroxylase (TH, Millipore, #AB152; 1:100)
132 to stain adrenergic nerve fibers and growth association protein 43 (GAP-43, Millipore,
133 #AB5220;1:100) for regenerating nerve terminals. Cardiac nerve fibers showed a regular
134 pattern along cardiomyocytes[24, 25]. Heart nerve endings density was quantified using
135 a square grid with 24 probes (area: 1 cm^2 each) overlapped to the digital images, which

136 were acquired using a Nikon Eclipse Ti fluorescence microscope with an 20x objective.
137 Five areas were randomly chosen for quantification from each of the three sections of
138 each sample. The total number of intercepts between nerve fibers and probes for each
139 area was assessed, and cardiac nerve fiber density was measured and expressed as the
140 mean number of intercepts per area (fibers/mm^2). A single operator assessed all the
141 measurements in a blinded manner. Next, to evaluate amyloid-β accumulation, 5- μm-
142 thick cardiac sections from each experimental group were marked with 6E10 anti-Aβ
143 antibody (Covance, SIG-39320, 1:500) and co-stained with cardiac troponin T (cTnT,
144 Thermo Scientific, #MA5-12960; 1:250), collagen type I (Rockland Immunochemicals,
145 #600-401-103-0.1; 1:100) or cleaved caspase-3 (Asp175) (Cl-Casp-3, Cell Signaling,
146 #94530; 1:200) antibodies. Nuclei were labeled with 4', 6-diamidino-2-phenylindole
147 (DAPI, Sigma Aldrich, D9542; 1:5000) and sections were mounted using an aqueous
148 mounting medium. Digital images were captured and analyzed by a Nikon Eclipse Ti
149 fluorescence microscope with 40x and 60x objectives. To evaluate vascular components,
150 after fixation, cardiac specimens were cut into 5-μm-thick longitudinal sections using a
151 freezing sliding microtome (Leica 2000R, Germany) (15723985). Next, tissue sections
152 were incubated for 30' minutes at 4°C in a blocking solution (10% donkey serum
153 supplemented with 0.3% Triton X-100 in phosphate-buffered saline). Via indirect
154 immunofluorescence procedure, sections were analyzed using rabbit polyclonal
155 antibodies against CD31 (AF3628- R&D Systems, 1:30) and α-smooth muscle actin (α-
156 SMA, ab32575- Abcam, 1:500) at 4°C overnight, followed by specific secondary
157 antibodies conjugated with cyanine 3 or cyanin 5 respectively, to stain vascular network.
158 For serum amyloid A3 immunostaining (SAA), fixed 5-μm-thick cardiac sections were
159 retrieved with formic acid 70% solution (Thermo Scientific, #270480010) for twenty
160 minutes at room temperature, next they were processed using rat monoclonal antibody
161 against SAA (Abcam, #ab231680; 1:50) and co-stained with rabbit polyclonal antibody
162 against fibronectin (Abcam, #ab2413; 1:100) for two hours at 37°C, followed by specific
163 secondary antibodies combined with Alexa Fluor 488-conjugated anti-rat IgG and Alexa
164 Fluor 555-conjugated anti-rabbit IgG, respectively. DAPI was used to counterstain nuclei,
165 and cardiac sections were mounted with a Vectashield vibrance antifade mounting
166 medium. Images were acquired and examined using a Nikon Eclipse Ti2 fluorescence

167 microscope with 20x and 40x objectives. A single operator blindly performed all the
168 procedures.

169 **2.5 Preparation of cell and tissue lysates and immunoblotting analysis**

170 Cellular and cardiac samples were homogenized using RIPA cell lysis buffer (Thermo
171 Scientific) enriched with phosphatases and protease inhibitors (Thermo Scientific). Then,
172 the lysates underwent sonication and were centrifuged for 10 min at 4°C at 13,000 rpm
173 to discard the insoluble debris. Next, total protein amounts were quantified via a dye-
174 binding Pierce BCA protein assay kit (Thermo Scientific) and detected using a
175 spectrophotometer reader (SpectraMax i3x Multi-mode Microplate Reader, Molecular
176 Devices) at a wavelength of 512 nm. Equal yields of protein (20-40 µg) were separated
177 through SDS-PAGE and identified by western blot analysis. Total lysates were used to
178 evaluate the protein levels of NGF (AN-240; Alomone labs; 1:1000), BDNF (ANT-010;
179 Alomone labs; 1:1000), GAP-43 (Millipore AB552; 1:1000), Cleaved Caspase-3- Asp175
180 (Cl-Casp-3- Cell Signaling- #94530; 1:200), dopamine β hydroxylase (DβH; AB1536;
181 Millipore), human Aβ [mouse monoclonal anti-Aβ antibodies mixture composed of 4G8
182 epitope (residues Aβ18-22; SIG-39320; Covance) and 6E10 epitope (residues Aβ3-8;
183 SIG-39220; Covance)], and GAPDH (sc-32233,6C5; Santa Cruz Biotechnology; 1: 2000),
184 the latter which was used as the loading control. Protein bands were detected by using
185 Odyssey® CLx Imaging System according to the manufacturer's instructions and
186 quantified with Image Studio™ Lite Software[26].

187 **2.6. ELISA**

188 Aβ40 and Aβ42 peptides levels were detected using a commercial ELISA kit (Invitrogen
189 KHB3481 and KHB3441, respectively). Briefly, cardiac specimens for each mouse were
190 collected at the end of the experimental study and homogenized with RIPA cell lysis buffer
191 (Thermo Scientific), supplemented with phosphatases and protease inhibitors (Thermo
192 Scientific, Waltham, MA). Then, ELISA was performed using an equal amount of total
193 cardiac protein following the company's specifications, and the plate was evaluated at
194 450 nm with a spectrophotometer reader (SpectraMax i3x Multi-mode Microplate Reader,
195 Molecular Devices).

196 **2.7. Cell culture and treatments**

197 Human cardiomyocytes (AC16, purchased from Millipore, #SCC109) were expanded in
198 10 cm^2 dishes in a humidified environment at 37°C with 5% CO2 in DMEM/F12 medium
199 (Lonza Ltd. Basel, Switzerland) supplemented with 12.5% fetal bovine serum (FBS) and
200 1% penicillin-streptomycin (P/S, Lonza). Human SH-SY5Y neuroblastoma cells (ATCC,
201 CRL-2266, a neuronal cell line used widely in experimental neurological studies), were
202 grown in 10 cm^2 dishes in a humidified environment at 37°C with 5% CO_2 in DMEM/F12
203 medium (Lonza Ltd. Basel, Switzerland) supplemented with 10% fetal bovine serum
204 (FBS) and 1% penicillin-streptomycin (P/S, Lonza). For both cell types, SH-SY5Y and
205 AC16, an equal number of cells were seeded in 6 well plates and, after 24h, cells were
206 challenged with human Aβ40 or Aβ42 oligomers for 16 hours.

207 **2.8. Aβ peptides**

208 Pre-aggregated Aβ40 and Aβ42 oligomers were generated from HFIP-treated and
209 lyophilized peptides as previously described[27, 28]. Briefly, oligomer enriched Aβ40 and
210 Aβ42 preparations were obtained after a dilution of the peptide in DMSO at a
211 concentration of 5 mM, then diluted to 100 μM in ice-cold DMEM/F12 media and
212 incubated at 4°C for 16 hours. Next, Aβ40 and Aβ42 oligomers were resuspended in
213 DMEM/F12 medium to 10 μM as a final concentration for the cell treatments.

214 **2.9. Statistical methods and analysis**

215 All *in vitro* and *in vivo* experiments during the study period were performed blindly. Data
216 are expressed as means ± SEM. Statistical significance between 2 groups was
217 determined by two-tailed Student's t-test. When comparing multiple groups, data were
218 analyzed using a one-way analysis of variance (ANOVA) test, followed by Tukey's post
219 hoc test. Differences between groups were considered statistically significant when
220 $p \leq 0.05$. All data were analyzed and graphically represented using GraphPad Prism
221 software version 9 (GraphPad, La Jolla, CA).

222

223

224 **3. Results**

225 **3.1. AD amyloid pathology impairs cardiac function and promotes myocardial**
226 **interstitial fibrosis.**

227 To evaluate the effects of AD amyloid pathology on cardiac tissue functionality and
228 systolic activity, LV function and cardiac chamber dimensions were determined by
229 echocardiographic analysis before or after the development of cerebral Aβ pathology (4-
230 or 12-months) in Tg2576 transgenic mice, a widely used model of cerebral amyloidosis,
231 and age-matched WT littermates (Study design in supplementary Fig.1). Bi-dimensional
232 M-mode tracings revealed a significant decrease in both, ejection fraction (EF%) and
233 fractional shortening (FS%) percentage of 12-month-old Tg2576 mice compared to WT
234 littermates (Fig. 1A-B). No significant changes were found in systolic function in young
235 (4month-old) Tg2576 mice (Supplementary Fig.1). Additionally, 12-month-old transgenic
236 mice showed a remarkable left ventricle enlargement, as evidenced by the increased left
237 ventricular end-systolic diameter (LVESD) (Fig.1A-B). The LV chamber dilation resulted
238 in a relevant increase in left ventricle volumes, expressed as left ventricular end-systolic
239 volume (LVESV) (Fig.1B). Differences in gravimetric parameters were confirmed by
240 measuring the heart weight/body weight ratio, which significantly increased in Tg2576
241 mice compared to the WT group (Fig.1C). This severe deterioration of systolic function
242 and increased cardiac mass in the 12-month-old Tg2576 mouse was associated with a
243 prominent increase in myocardial interstitial fibrosis, as detected by Picrosirius red
244 staining (Fig.1D-E). Overall, these findings suggest that AD pathology causes detrimental
245 effects on systolic function and parenchymal tissue structure of the heart.

246 **3.2. AD increases Aβ accumulation within the myocardial parenchyma in**
247 **association with apoptosis.**

248 Recently, a clinical report demonstrated the presence of Aβ deposits in the myocardial
249 tissue of patients affected by AD, resulting in a progressive diastolic impairment[10]. In
250 line with this, our data revealed a degradation of the extracellular matrix with increased
251 collagen deposition and Aβ40 accumulation, the latter quantified by ELISA, in 12-month-
252 old Tg2576 cardiac tissue compared to the WT group (Fig. 2A). Intriguingly, no changes

253 in Aβ42 levels were observed between the WT and Tg2576 groups (Fig.2B). These
254 results are consistent with the age-dependent production of Aβ peptides in the Tg2576
255 mouse model, which exhibits higher abundance and a progressive increase in cerebral
256 Aβ40 levels compared to Aβ42[29]. The cardiac Aβ40 deposition evidenced by ELISA
257 was validated by western blot analysis, which confirmed a significant increase of Aβ
258 dimers and oligomers in total heart lysates of Tg2576 as opposed to WT littermates (Fig.
259 2C-D). Interestingly, the immunofluorescence staining revealed that amyloid aggregates
260 accumulate in the interstitial spaces between cardiomyocytes, together with collagen type
261 I fibers (Fig. 2F-G, *top panels*), thus corroborating the myocardial interstitial fibrosis
262 evidenced by Picro-sirius red staining. Aβ accumulation is known to cause increase in
263 apoptosis in vascular and neuronal cells and in AD brains, as well as in cardiac cells in
264 culture [30-34]. Indeed, analysis of the cardiac tissue by WB and IHC revealed
265 upregulation of cleaved-caspase 3 levels in Tg2576 hearts (Fig.2C-E, and F-G). In
266 summary, these data suggest that the accumulation of Aβ in the myocardial interstitium
267 results in cardiac cell apoptosis and dysfunction.

268 **3.3. Amyloid-β pathology induces misfolding of serum amyloid A3 and its**
269 **deposition in the cardiac vessel walls.**

270 Protein misfolding diseases, including AD, are characterized by a progressive
271 derangement in protein organization, during which seeding processes may be triggered
272 by different forms of amyloid interacting with each other[35]. It is therefore conceivable
273 that the progressive accumulation of misfolded Aβ oligomers in the heart tissue may result
274 in both, a significant increase in fibrosis and the seeding of other amyloid peptides such
275 as serum amyloid A (SAA) proteins. SAAs belong to the apolipoproteins category,
276 associated with inflammatory stimuli and activation of enzymes involved in extracellular
277 matrix deterioration[36]. High levels of SAAs proteins usually do not lead to fibrillar
278 deposits. However, a chronic inflammatory state, or a seeding process (such as that
279 promoted by Aβ), may induce these SAAs peptides to accumulate in peripheral tissues.
280 Indeed, we found accumulation of Aβ aggregates around cardiac vessels in the Tg2576
281 mice, with infiltration of the vascular basal lamina (Fig.3 and Supplementary Fig.2D),
282 which was accompanied by an increase of serum amyloid A3 (SAA3) vascular deposits

283 (Fig 4A). As confirmed by immunoblot analysis, SAA3 dimers were increased in the
284 cardiac tissue of Tg mice (Fig.4B). This accumulation and promoted aggregation of serum
285 amyloid proteins may further contribute to the impairment of cardiac function and to the
286 fibrotic phenotype.
287

288 **3.4. Aβ pathology severely impacts neurotrophic signaling in the brain and heart.**

289 AD pathology and Aβ deposition significantly impair the production of neurotrophins in
290 the brain, leading to a progressive loss of the two major neuromodulators, NGF and
291 BDNF, thus contributing to cognitive impairment and dementia[37, 38]. However, whether
292 AD pathology can modulate peripheral neurotrophic activity and cardiac innervation
293 remains to be elucidated. Therefore, we explored the regulation of neuro-signaling
294 modulators and innervation factors both in the cerebral cortex and cardiac lysates of 12-
295 month-old Tg2576 mice. Immunoblotting analysis showed a robust decline in both
296 cerebral and cardiac levels of NGF and BDNF expression in the Tg2576 group compared
297 to WT mice (Fig.5 A-B). This decrease in the levels of neurotrophins exhibited by
298 transgenic mice was associated with a relevant reduction in the adrenergic marker (DβH)
299 and in the neuronal fibers' regeneration marker, GAP-43 (Fig.4A-B). Interestingly, IHC
300 analysis confirmed an evident loss in cardiac nerve fibers density in Tg2576 mice
301 compared to WT animals, including both sympathetic and regenerating nerve endings,
302 labeled with TH and GAP-43 markers, respectively (Fig.5 C-D). Taken together, these
303 results indicate that AD amyloid pathology also results in harmful effects on peripheral
304 neurotrophic pathways, hence impacting the peripheral nervous system and cardiac
305 innervation.

306 **3.5. Aβ oligomers impair neurotrophins production in cardiomyocytes and**
307 **neuroblastoma cells.**

308 Our *in vivo* studies in Tg2576 mice, a widely used AD model, demonstrated a remarkable
309 reduction of neurotrophic markers and nerve fibers within the cardiac tissue. To
310 demonstrate that this loss of NTFs is caused by Aβ aggregates that accumulate in the
311 heart, we assessed the effects of Aβ40 oligomers, known as the most toxic aggregation
312 species, on the production of neurotrophins and neuronal regeneration markers in human

313 cardiomyocytes and neuronal SH-SY5Y cells (Fig.6- 7). In addition to Aβ40, Aβ42 effects
314 were also tested in SH-SY5Y cells, since neurons are typically exposed to both peptides.
315 Incubation of the cells for 16 hours with Aβ peptides significantly reduced protein levels
316 of GAP-43 and BDNF in neuronal cells compared with the non-treated group, with no
317 significant changes in NGF expression (Fig.6), and significantly reduced the expression
318 of BDNF in cardiomyocytes (Fig. 7). These data support the hypothesis that amyloid
319 aggregates are, at least in part, responsible for the impairment of the cardiac neuro-
320 signaling pathway and neuronal regeneration, particularly by reducing the production of
321 BDNF in both neurons and cardiomyocytes and the levels of GAP-43 in neurons.

322 **4. Discussion**

323 This study demonstrates for the first time a severe cardiac functional, morphological, and
324 neurotrophic impairment in the Tg2576 mice, a widely used animal model of cerebral
325 amyloidosis and AD. These alterations include dramatically reduced EF% and FS%,
326 increased LV volume and heart weight. Our data suggests that cardiac amyloidosis
327 (including Aβ and SAA3 deposition) promotes interstitial fibrosis and a loss of cardiac
328 innervation, neurotrophins and neuro-signaling pathway impairment, which appear to be
329 essential mediators of the observed cardiac dysfunction. Importantly, these findings are
330 consistent with recent clinical studies that showed cardiac defects and Aβ accumulation
331 in the hearts of AD patients [10, 39].
332 The heart-brain axis constitutes a complex and highly regulated bi-directional
333 interconnection between the central and peripheral nervous systems[40, 41].
334 Neurodegenerative pathologies, such as AD, through the modulation of both the central
335 and the peripheral nervous system, may have serious and debilitating effects on multiple
336 peripheral organs, including the heart. However, the effects of AD pathology and Aβ
337 accumulation in the heart of AD patients and animal models have not been clearly
338 elucidated. Age-related heart-brain axis remodeling increases the susceptibility to both
339 neurodegenerative and chronic cardiac disorders, thus leading to a raise in morbidities
340 and mortality risk[42-44]. An increasing number of studies are starting to highlight the
341 involvement of the cardiac tissue in neurodegenerative diseases, revealing a compelling
342 interplay between AD and cardiac disorders, such as atrial fibrillation[45], heart failure[46-

343 48], and coronary artery disease[49, 50]. It has been recently shown that AD patients
344 exhibit myocardial dysfunction following the deposition of Aβ aggregates in the cardiac
345 tissue[10]. In line with this, Sanna and coworkers described the presence of structural
346 and functional abnormalities (diastolic impairment, ECG alterations, and interventricular
347 septum thickness enhancement) in the cardiac tissue of a small cohort of AD subjects[6].
348 Interestingly, short N-terminal cleavage products of APP were found in the myocardium.
349 Their frequency correlated with age, degree of myocardial fibrosis in individuals with
350 hypertension and with the severity of cerebral amyloid angiopathy (CAA), suggesting a
351 link between cerebrovascular and cardiac APP-related amyloidosis[39]. AD pathology
352 has been shown to severely impact the production and release of the main neurotrophic
353 factors, NGF and BDNF, in the brain[37, 51, 52]. These two neurotrophins are mainly
354 involved in the maturation and differentiation of neurons, ensuring neurogenesis and
355 synaptogenesis[53, 54]. The progressive decline in neurotrophic factor expression
356 observed in aging and exacerbated by AD pathology may lead to an adverse remodeling
357 of the neuro-signaling pathway, driving, together with other AD pathological factors, a
358 possible impairment of the peripheral innervation[38].
359 This study is the first to directly demonstrate, in a transgenic model of AD with CAA, the
360 effect of Aβ pathology on cardiac physiology, heart tissue dysfunction and cardiac cell
361 death, showing their association with peripheral innervation impairment and loss of
362 neurotrophins, such as BDNF and NGF. Since both cerebral parenchymal amyloid
363 pathology and CAA have been well described in the Tg2576 mice (e.g., progressive age-
364 dependent accumulation of Aβ aggregates in the brain parenchyma as well as in the brain
365 vasculature), we decided to assess whether a progressive impairment of cardiac
366 morphology and function was evident in this AD transgenic murine model[20, 55, 56]. We
367 found that Tg2576 mice show an age- dependent deterioration in cardiac systolic function
368 and a gradual replacement of viable myocardium with collagen fibers, together with a
369 progressive alteration of the extracellular matrix resulting in severe interstitial fibrosis (Fig.
370 1). This cardiac maladaptive remodeling is accompanied by a significant accumulation of
371 Aβ, particularly Aβ40, colocalized in perivascular and interstitial spaces with collagen
372 deposits, as well as caspase 3 activation in cardiomyocytes, suggesting that Aβ
373 deposition in the heart tissue contributes to the development of interstitial fibrosis and

374 apoptotic cardiac cell death (Fig. 2). The preferential accumulation of Aβ40, rather than
375 Aβ42, in Tg2576 mice hearts, is in line with previous studies describing the progressive
376 increase mostly of Aβ40 levels in both serum and brain parenchyma of Tg2576 mice
377 during aging[29]. In addition, the Aβ40 peptide is preferentially associated with vascular
378 deposits and CAA in the human brain, resulting in degenerative phenotypes in cerebral
379 endothelial cells[31], which culminate in vessel wall dysfunction[57, 58], contributing to
380 BBB permeability and microhemorrhages[59, 60]. This BBB dysfunction in AD brains may
381 enhance the systemic propagation of Aβ (including aggregated forms such as oligomers)
382 through the blood and its accumulation in peripheral organs, including the heart. Aβ40 is
383 the most abundant peptide in the cerebrospinal fluid and blood of AD patients as well as
384 in this mouse model and multiple biomarker studies have shown that this peptide does
385 not decrease in peripheral organs and tissues with AD progression[61]. Conversely, as
386 Aβ42 fibrils deposit in the brain parenchyma, Aβ42 levels decrease in the cerebrospinal
387 fluid and in the peripheral blood[62].
388 Aβ oligomers may also act as "seeds"[63], to induce aggregation of other amyloids, such
389 as SAA3 (as shown by our data), thus leading to extracellular matrix protein accumulation
390 in the heart and progressive cardiac impairment. At the molecular level, dysregulation
391 and misfolding of amyloid peptides induce a progressive rearranging of protein structure,
392 with seeding of other amyloids, gradually precipitating in the tissue parenchyma[64]. This
393 process characterizes a wide array of human diseases, including AD and CAA[35]. Some
394 of these aggregation species fuel cell stress and inflammation, resulting in degenerative
395 processes in multiple cell types, including endothelial and cardiac cells[30, 57, 58, 65-67].
396 We propose that this amyloid cross-seeding process progressively induces cardiac SAA3
397 apolipoproteins deposition in Tg2576 mice, culminating in significant extracellular matrix
398 deterioration and fibrosis[36]. Notably, SAA3 aggregates, together with Aβ deposits,
399 accumulated primarily around cardiac vessels (Fig. 3- 4), suggesting that misfolded Aβ
400 peptides or oligomers may diffuse through the vascular system, with consequential
401 seeding of other amyloids around the myocardial vessels. This evidence suggests that
402 the progressive deposition of amyloids in the cardiac tissue may initiate the observed
403 cardiac cell death, extracellular matrix alterations, heart fibrosis, cardiac dysfunction, and
404 the rarefaction of cardiac nerve fibers.

405 It is conceivable that, in this model, contractile dysfunction due to amyloid-mediated
406 cardiomyocytes cell death and neuronal dysregulation may proceed simultaneously or
407 that one may precede the other. As we have shown in cardiomyocytes and coronary
408 endothelial cells, as well as in cerebral endothelial cells, Aβ challenge plays a causal role
409 in inducing mitochondrial dysfunction and increased ROS production [27, 30], through
410 diminished energy metabolism, resulting in cardiac and endothelial cell dysfunction and
411 death. This cascade of events is likely to lead to the loss of cardiac cells, hypertrophy,
412 and deteriorated peripheral neurotrophic pathways in the heart. Specifically, we observed
413 a marked depletion in both adrenergic nerve endings and regenerated nerve terminals in
414 transgenic mouse hearts (Fig.5). This myocardial denervation was associated with a
415 robust reduction of both neurotrophic factors, NGF and BDNF, at the cerebral and cardiac
416 level, accompanied by significant impairment in the neuronal sprouting marker GAP-43
417 (Fig. 5). In AD patients, the decline of neuromodulators in the brain accelerates the age-
418 related synaptic loss, resulting in cognitive impairment[48, 68]. This process starts in the
419 early stages of AD pathology, worsening due to cellular and metabolic modifications,
420 pinnacling in a dramatic loss of neurons, synaptic rarefaction, and brain atrophy[69-71].
421 NTFs are powerful biomolecules with significant pleiotropic effects involved in cellular
422 growth and survival pathways, both in the brain and on cells/tissues outside the brain,
423 including endothelial cells, muscle cells, and the cardiovascular system[17, 72-74]. Here,
424 we demonstrated that Tg2576 mice exhibit a marked downregulation of the neuro
425 signaling pathway in both the brain and the heart. Thus, akin to elderly individuals and
426 heart failure subjects, AD patients may also be more exposed to cardiac impairment
427 because of neuronal signaling dysregulation, which may be both a consequence of
428 myocardial amyloid deposition, as well as of neurotrophic signaling impairment in
429 neuronal and cardiac cells. Notably, we observed that after treatment with Aβ oligomers,
430 BDNF and GAP-43 expression in human neuroblastoma SH-SY5Y cells and
431 cardiomyocytes (Fig. 6- 7) were considerably reduced. These findings suggest a direct
432 effect of Aβ on the reduction of NTFs in neurons, including those innervating the heart,
433 and in cardiac cells (Fig.6) and represents the first report of an Aβ-induced reduction in
434 neurotrophic factors in cardiomyocytes.

435 Since neurotrophic factors are also involved in angiogenesis and relaxation/contraction
436 coupling processes, their deficit sharply impairs cardiac function[75, 76]. In this regard,
437 the observed loss of BDNF and NGF is likely to be a key contributor to the cardiac
438 pathological state observed in our AD model, providing additional clarification on the
439 reasons why AD patients may be more prone to develop cardiovascular disorders of
440 different etiology[77, 78]. The decline in NGF and BDNF in the Tg2576 animals was
441 associated with a downregulation of TH and GAP-43, confirming the rarefaction of cardiac
442 nerve fibers, and the impairment of their neuronal regeneration capability.
443 Aβ challenge may also have additional toxic effects on cardiac cells. As we have recently
444 demonstrated, Aβ reduced cell survival and increased mitochondrial swelling and ROS
445 production on H9c2 cardio-myoblasts and human coronary artery endothelial cells[30].
446 This is in line with the current findings showing an increased activation of caspase-3 in
447 cardiac cells of Tg2576 mice.
448 Collectively, our novel findings suggest that AD pathology could be responsible for
449 structural and functional alterations in the heart, including deficits in the cardiac nervous
450 system, as previously shown for aging and heart failure[15, 17, 25].
451
452 **4.1 Limitations.** The present study is not free of limitations. First, larger longitudinal
453 studies involving heart IHC and biochemistry at many stages of AD pathology in mouse
454 models and humans will be needed to demonstrate whether amyloidosis and loss of
455 cardiac innervation are simultaneous, or if one precedes the other. Also, we did not
456 investigate LV diastolic function in our *in ²vivo* model. Previous investigations have
457 demonstrated diastolic impairment correlated with cardiac electric abnormalities in a small
458 group of AD patients. Here, we confirmed cardiac dysfunction through systolic
459 evaluations. Our investigation of the neuro-signaling pathway may miss other
460 neurotrophins involved in cardiac function such as NT3 and NT4. In this study, we focused
461 on the two main neuromodulators (NGF and BDNF), which are well-characterized and
462 accountable for regulating and preserving the brain/heart axis equilibrium. Additionally, it
463 cannot be excluded that this transgenic model may involve the production of Aβ by
464 peripheral neurons. However, this reflects the case of human aging and AD patients, in
465 which the production of Aβ may be expected also in peripheral neuronal cells, and overall

466 clearance mechanisms are compromised by aging. In fact, the validity and clinical
467 relevance of our findings is confirmed by the presence of Aβ deposits in the heart of AD
468 patients[10]. Lastly, future investigations are needed to better elucidate the mechanisms
469 responsible for the cardiac neuro-signaling impairment and loss of nerve terminals that
470 occurs in Alzheimer's pathology. Our *in vitro* data suggests that Aβ is, at least in part,
471 causal for these effects.
472
473 **4.2 Conclusions.** Overall, our findings reveal a maladaptive remodeling induced by AD
474 amyloid pathology on the heart, with Aβ and SAA3 amyloid deposition, fibrosis, and
475 neurotrophic signaling pathway dysregulation, resulting in an important impairment of
476 cardiac function. This progressive brain/heart axis deterioration is very likely to increase
477 the risk of developing cardiovascular disorders in AD patients. The discovery of these
478 previously uninvestigated AD-mediated myocardial pathological mechanisms, in addition
479 to improving our knowledge on the peripheral implications of AD, provides novel
480 appealing therapeutic targets, such as the neurotrophic signaling pathway, to delay the
481 harmful changes induced by AD and amyloid pathology on the cardiovascular system.

482 **5. Funding**

483 This work was supported by NIH R01NS104127 and R01AG062572 grants, the
484 Alzheimer's Association (AARG-20-685663), the Pennsylvania Department of Heath
485 Collaborative Research on Alzheimer's Disease (PA Cure) Grant, awarded to SF, by the
486 NIH SC1GM128210 grant awarded to SJ, and by the Karen Toffler Charitable Trust, and
487 the Lemole Center for Integrated Lymphatics research.

488 **6. Authors Contribution**

489 AE and SF designed the study. AE performed and conceptualized the experiments and
490 analyzed the data. AE wrote the paper draft and did the literature search. RPR, AC and
491 RVT performed experiments. SF provided relevant insights and scientific supervision. SJ
492 and SF critically revised the study, edited the manuscript, provided additional literature
493 search, and acquired funding.

494 **7. Conflict of interest**

The authors declare no conflicts of interest.

8. Data availability

The data underlying this article will be shared on reasonable request to the corresponding author.

9. References

1. Hebert, L.E., et al., *Alzheimer disease in the United States (2010-2050) estimated using the 2010 census.* Neurology, 2013. **80**(19): p. 1778-83.
2. Masters, C.L., et al., *Alzheimer's disease.* Nat Rev Dis Primers, 2015. **1**: p. 15056.
3. Castellani, R.J., R.K. Rolston, and M.A. Smith, *Alzheimer disease.* Dis Mon, 2010. **56**(9): p. 484-546.
4. Fratiglioni, L., D. De Ronchi, and H. Aguero-Torres, *Worldwide prevalence and incidence of dementia.* Drugs Aging, 1999. **15**(5): p. 365-75.
5. Small, G.W., et al., *Diagnosis and treatment of Alzheimer disease and related disorders. Consensus statement of the American Association for Geriatric Psychiatry, the Alzheimer's Association, and the American Geriatrics Society.* JAMA, 1997. **278**(16): p. 1363-71.
6. Sanna, G.D., et al., *Cardiac Abnormalities in Alzheimer Disease: Clinical Relevance Beyond Pathophysiological Rationale and Instrumental Findings?* JACC Heart Fail, 2019. **7**(2): p. 121-128.
7. Paciaroni, M. and J. Bogousslavsky, *Connecting cardiovascular disease and dementia: further evidence.* J Am Heart Assoc, 2013. **2**(6): p. e000656.
8. Tini, G., et al., *Alzheimer's Disease and Cardiovascular Disease: A Particular Association.* Cardiol Res Pract, 2020. **2020**: p. 2617970.
9. Yang, M., et al., *Interrelationship between Alzheimer's disease and cardiac dysfunction: the brain-heart continuum?* Acta Biochim Biophys Sin (Shanghai), 2020. **52**(1): p. 1-8.
10. Troncone, L., et al., *Abeta Amyloid Pathology Affects the Hearts of Patients With Alzheimer's Disease: Mind the Heart.* J Am Coll Cardiol, 2016. **68**(22): p. 2395-2407.

526 11. Gianni, D., et al., *Protein aggregates and novel presenilin gene variants in*
527 *idiopathic dilated cardiomyopathy.* Circulation, 2010. **121**(10): p. 1216-26.
528 12. Li, D., et al., *Mutations of presenilin genes in dilated cardiomyopathy and heart*
529 *failure.* Am J Hum Genet, 2006. **79**(6): p. 1030-9.
530 13. Allen, S.J., J.J. Watson, and D. Dawbarn, *The neurotrophins and their role in*
531 *Alzheimer's disease.* Curr Neuropharmacol, 2011. **9**(4): p. 559-73.
532 14. Garzon, D., G. Yu, and M. Fahnestock, *A new brain-derived neurotrophic factor*
533 *transcript and decrease in brain-derived neurotrophic factor transcripts 1, 2 and 3*
534 *in Alzheimer's disease parietal cortex.* J Neurochem, 2002. **82**(5): p. 1058-64.
535 15. Poon, W.W., et al., *beta-Amyloid (Abeta) oligomers impair brain-derived*
536 *neurotrophic factor retrograde trafficking by down-regulating ubiquitin C-terminal*
537 *hydrolase, UCH-L1.* J Biol Chem, 2013. **288**(23): p. 16937-16948.
538 16. Zheng, Z., B. Sabirzhanov, and J. Keifer, *Oligomeric amyloid-beta inhibits the*
539 *proteolytic conversion of brain-derived neurotrophic factor (BDNF), AMPA receptor*
540 *trafficking, and classical conditioning.* J Biol Chem, 2010. **285**(45): p. 34708-17.
541 17. Elia, A., et al., *Aging is associated with cardiac autonomic nerve fiber depletion*
542 *and reduced cardiac and circulating BDNF levels.* J Geriatr Cardiol, 2021. **18**(7):
543 p. 549-559.
544 18. Halade, G.V., et al., *Reduced BDNF attenuates inflammation and angiogenesis to*
545 *improve survival and cardiac function following myocardial infarction in mice.* Am
546 J Physiol Heart Circ Physiol, 2013. **305**(12): p. H1830-42.
547 19. Hiltunen, J.O., et al., *Nerve growth factor and brain-derived neurotrophic factor*
548 *mRNAs are regulated in distinct cell populations of rat heart after ischaemia and*
549 *reperfusion.* J Pathol, 2001. **194**(2): p. 247-53.
550 20. Hsiao, K., et al., *Correlative memory deficits, Abeta elevation, and amyloid plaques*
551 *in transgenic mice.* Science, 1996. **274**(5284): p. 99-102.
552 21. Robbins, E.M., et al., *Kinetics of cerebral amyloid angiopathy progression in a*
553 *transgenic mouse model of Alzheimer disease.* J Neurosci, 2006. **26**(2): p. 365-71.
554 22. Rigaud, V.O., et al., *UCP2 modulates cardiomyocyte cell cycle activity, acetyl-CoA,*
555 *and histone acetylation in response to moderate hypoxia.* JCI Insight, 2022. **7**(15).

556 23. Cannavo, A., et al., *Aldosterone Jeopardizes Myocardial Insulin and beta-*
557 *Adrenergic Receptor Signaling via G Protein-Coupled Receptor Kinase 2.* Front
558 Pharmacol, 2019. **10**: p. 888.
559 24. de Lucia, C., et al., *Long-Term Caloric Restriction Improves Cardiac Function,*
560 *Remodeling, Adrenergic Responsiveness, and Sympathetic Innervation in a Model*
561 *of Postischemic Heart Failure.* Circ Heart Fail, 2018. **11**(3): p. e004153.
562 25. Parisi, V., et al., *Increased Epicardial Adipose Tissue Volume Correlates With*
563 *Cardiac Sympathetic Denervation in Patients With Heart Failure.* Circ Res, 2016.
564 **118**(8): p. 1244-53.
565 26. Marzano, F., et al., *Genetic Catalytic Inactivation of GRK5 Impairs Cardiac*
566 *Function in Mice Via Dysregulated P53 Levels.* JACC Basic Transl Sci, 2022. **7**(4):
567 p. 366-380.
568 27. Fossati, S., et al., *The carbonic anhydrase inhibitor methazolamide prevents*
569 *amyloid beta-induced mitochondrial dysfunction and caspase activation protecting*
570 *neuronal and glial cells in vitro and in the mouse brain.* Neurobiol Dis, 2016. **86**: p.
571 29-40.
572 28. Stine, W.B., Jr., et al., *In vitro characterization of conditions for amyloid-beta*
573 *peptide oligomerization and fibrillogenesis.* J Biol Chem, 2003. **278**(13): p. 11612-
574 22.
575 29. Kawarabayashi, T., et al., *Age-dependent changes in brain, CSF, and plasma*
576 *amyloid (beta) protein in the Tg2576 transgenic mouse model of Alzheimer's*
577 *disease.* J Neurosci, 2001. **21**(2): p. 372-81.
578 30. Jang, S., et al., *Beta-Amyloid Instigates Dysfunction of Mitochondria in Cardiac*
579 *Cells.* Cells, 2022. **11**(3).
580 31. Parodi-Rullan, R., et al., *Alzheimer's amyloid beta heterogeneous species*
581 *differentially affect brain endothelial cell viability, blood-brain barrier integrity, and*
582 *angiogenesis.* Aging Cell, 2020. **19**(11): p. e13258.
583 32. Kim, J., et al., *Beta-amyloid oligomers activate apoptotic BAK pore for cytochrome*
584 *c release.* Biophys J, 2014. **107**(7): p. 1601-8.

585 33. Fossati, S., J. Ghiso, and A. Rostagno, *TRAIL death receptors DR4 and DR5*
586 *mediate cerebral microvascular endothelial cell apoptosis induced by oligomeric*
587 *Alzheimer's Abeta.* Cell Death Dis, 2012. **3**: p. e321.
588 34. Eckert, A., et al., *Increased apoptotic cell death in sporadic and genetic*
589 *Alzheimer's disease.* Ann N Y Acad Sci, 2003. **1010**: p. 604-9.
590 35. Dobson, C.M., *Principles of protein folding, misfolding and aggregation.* Semin Cell
591 Dev Biol, 2004. **15**(1): p. 3-16.
592 36. Uhlar, C.M. and A.S. Whitehead, *Serum amyloid A, the major vertebrate acute-*
593 *phase reactant.* Eur J Biochem, 1999. **265**(2): p. 501-23.
594 37. Arancio, O. and M.V. Chao, *Neurotrophins, synaptic plasticity and dementia.* Curr
595 Opin Neurobiol, 2007. **17**(3): p. 325-30.
596 38. Nasrolahi, A., et al., *Therapeutic potential of neurotrophic factors in Alzheimer's*
597 *Disease.* Mol Biol Rep, 2022. **49**(3): p. 2345-2357.
598 39. Kramer, L.M., et al., *Amyloid precursor protein-fragments-containing inclusions in*
599 *cardiomyocytes with basophilic degeneration and its association with cerebral*
600 *amyloid angiopathy and myocardial fibrosis.* Sci Rep, 2018. **8**(1): p. 16594.
601 40. Samuels, M.A., *The brain-heart connection.* Circulation, 2007. **116**(1): p. 77-84.
602 41. Tahsili-Fahadan, P. and R.G. Geocadin, *Heart-Brain Axis: Effects of Neurologic*
603 *Injury on Cardiovascular Function.* Circ Res, 2017. **120**(3): p. 559-572.
604 42. Daniele, G., et al., *Heart and Brain: Complex Relationships for Left Ventricular*
605 *Dysfunction.* Curr Cardiol Rep, 2020. **22**(8): p. 72.
606 43. Hooghiemstra, A.M., et al., *Frequent Cognitive Impairment in Patients With*
607 *Disorders Along the Heart-Brain Axis.* Stroke, 2019. **50**(12): p. 3369-3375.
608 44. Veugen, M.G.J., et al., *Cross-Sectional Associations Between Cardiac*
609 *Biomarkers, Cognitive Performance, and Structural Brain Changes Are Modified*
610 *by Age.* Arterioscler Thromb Vasc Biol, 2018. **38**(8): p. 1948-1958.
611 45. Ihara, M. and K. Washida, *Linking Atrial Fibrillation with Alzheimer's Disease:*
612 *Epidemiological, Pathological, and Mechanistic Evidence.* J Alzheimers Dis, 2018.
613 **62**(1): p. 61-72.
614 46. Cermakova, P., et al., *Heart failure and Alzheimer's disease.* J Intern Med, 2015.
615 **277**(4): p. 406-25.

616 47. Cohen, M.B. and P.J. Mather, *A review of the association between congestive*
617 *heart failure and cognitive impairment.* Am J Geriatr Cardiol, 2007. **16**(3): p. 171-
618 4.
619 48. Hoth, K.F., et al., *Cardiac dysfunction and cognition in older adults with heart*
620 *failure.* Cogn Behav Neurol, 2008. **21**(2): p. 65-72.
621 49. Roger, V.L., *Epidemiology of heart failure.* Circ Res, 2013. **113**(6): p. 646-59.
622 50. Tublin, J.M., et al., *Getting to the Heart of Alzheimer Disease.* Circ Res, 2019.
623 **124**(1): p. 142-149.
624 51. Cade, S., X.F. Zhou, and L. Bobrovskaya, *The role of brain-derived neurotrophic*
625 *factor and the neurotrophin receptor p75NTR in age-related brain atrophy and the*
626 *transition to Alzheimer's disease.* Rev Neurosci, 2022. **33**(5): p. 515-529.
627 52. Gao, L., et al., *Brain-derived neurotrophic factor in Alzheimer's disease and its*
628 *pharmaceutical potential.* Transl Neurodegener, 2022. **11**(1): p. 4.
629 53. Vitaliano, G.D., et al., *Clathrin-nanoparticles deliver BDNF to hippocampus and*
630 *enhance neurogenesis, synaptogenesis and cognition in HIV/neuroAIDS mouse*
631 *model.* Commun Biol, 2022. **5**(1): p. 236.
632 54. Wang, C.S., E.T. Kavalali, and L.M. Monteggia, *BDNF signaling in context: From*
633 *synaptic regulation to psychiatric disorders.* Cell, 2022. **185**(1): p. 62-76.
634 55. Irizarry, M.C., et al., *APPSw transgenic mice develop age-related A beta deposits*
635 *and neuropil abnormalities, but no neuronal loss in CA1.* J Neuropathol Exp
636 Neurol, 1997. **56**(9): p. 965-73.
637 56. Jung, J.H., et al., *Pathway-specific alteration of synaptic plasticity in Tg2576 mice.*
638 Mol Cells, 2011. **32**(2): p. 197-201.
639 57. Fossati, S., et al., *Differential activation of mitochondrial apoptotic pathways by*
640 *vasculotropic amyloid-beta variants in cells composing the cerebral vessel walls.*
641 FASEB J, 2010. **24**(1): p. 229-41.
642 58. Fossati, S., J. Ghiso, and A. Rostagno, *TRAIL death receptors DR4 and DR5*
643 *mediate cerebral microvascular endothelial cell apoptosis induced by oligomeric*
644 *Alzheimer's Abeta.* Cell Death Dis, 2012. **3**(6): p. e321.

645 59. Ghiso, J., S. Fossati, and A. Rostagno, *Amyloidosis associated with cerebral*
646 *amyloid angiopathy: cell signaling pathways elicited in cerebral endothelial cells.* J
647 Alzheimers Dis, 2014. **42 Suppl 3**(0 3): p. S167-76.
648 60. Lemon, N., et al., *Carbonic Anhydrases as Potential Targets Against*
649 *Neurovascular Unit Dysfunction in Alzheimer's Disease and Stroke.* Front Aging
650 Neurosci, 2021. **13**: p. 772278.
651 61. Hanon, O., et al., *Plasma amyloid beta predicts conversion to dementia in subjects*
652 *with mild cognitive impairment: The BALTAZAR study.* Alzheimers Dement, 2022.
653 62. Zicha, S., et al., *Comparative analytical performance of multiple plasma Abeta42*
654 *and Abeta40 assays and their ability to predict positron emission tomography*
655 *amyloid positivity.* Alzheimers Dement, 2022.
656 63. Ulm, B.S., D.R. Borchelt, and B.D. Moore, *Remodeling Alzheimer-amyloidosis*
657 *models by seeding.* Mol Neurodegener, 2021. **16**(1): p. 8.
658 64. Lyubchenko, Y.L., *Amyloid misfolding, aggregation, and the early onset of protein*
659 *deposition diseases: insights from AFM experiments and computational analyses.*
660 AIMS Mol Sci, 2015. **2**(3): p. 190-210.
661 65. Fossati, S., J. Ghiso, and A. Rostagno, *Insights into caspase-mediated apoptotic*
662 *pathways induced by amyloid-beta in cerebral microvascular endothelial cells.*
663 Neurodegener Dis, 2012. **10**(1-4): p. 324-8.
664 66. Parodi-Rullan, R., J.Y. Sone, and S. Fossati, *Endothelial Mitochondrial*
665 *Dysfunction in Cerebral Amyloid Angiopathy and Alzheimer's Disease.* J
666 Alzheimers Dis, 2019. **72**(4): p. 1019-1039.
667 67. Parodi-Rullan, R.M., S. Javadov, and S. Fossati, *Dissecting the Crosstalk between*
668 *Endothelial Mitochondrial Damage, Vascular Inflammation, and*
669 *Neurodegeneration in Cerebral Amyloid Angiopathy and Alzheimer's Disease.*
670 Cells, 2021. **10**(11).
671 68. Numakawa, T. and H. Odaka, *The Role of Neurotrophin Signaling in Age-Related*
672 *Cognitive Decline and Cognitive Diseases.* Int J Mol Sci, 2022. **23**(14).
673 69. O'Leary, T.P. and R.E. Brown, *Visuo-spatial learning and memory impairments in*
674 *the 5xFAD mouse model of Alzheimer's disease: Effects of age, sex, albinism, and*
675 *motor impairments.* Genes Brain Behav, 2022. **21**(4): p. e12794.

676 70. Paasila, P.J., et al., *Synapses, Microglia, and Lipids in Alzheimer's Disease.* Front
677 Neurosci, 2021. **15**: p. 778822.
678 71. Urayama, A., et al., *Preventive and therapeutic reduction of amyloid deposition*
679 *and behavioral impairments in a model of Alzheimer's disease by whole blood*
680 *exchange.* Mol Psychiatry, 2022. **27**(10): p. 4285-4296.
681 72. Daquinag, A.C., et al., *Endothelial TrkA coordinates vascularization and*
682 *innervation in thermogenic adipose tissue and can be targeted to control*
683 *metabolism.* Mol Metab, 2022. **63**: p. 101544.
684 73. Fang, C.N., et al., *NGF/TrkA promotes the vitality, migration and adhesion of bone*
685 *marrow stromal cells in hypoxia by regulating the Nrf2 pathway.* Metab Brain Dis,
686 2022. **37**(6): p. 2017-2026.
687 74. Pius-Sadowska, E. and B. Machalinski, *BDNF - A key player in cardiovascular*
688 *system.* J Mol Cell Cardiol, 2017. **110**: p. 54-60.
689 75. Abcejo, A.J., et al., *Brain-derived neurotrophic factor enhances calcium regulatory*
690 *mechanisms in human airway smooth muscle.* PLoS One, 2012. **7**(8): p. e44343.
691 76. Cannavo, A., et al., *beta3AR-Dependent Brain-Derived Neurotrophic Factor*
692 *(BDNF) Generation Limits Chronic Postischemic Heart Failure.* Circ Res, 2023.
693 **132**(7): p. 867-881.
694 77. Bahls, M., et al., *Brain-derived neurotrophic factor is related with adverse cardiac*
695 *remodeling and high NTproBNP.* Sci Rep, 2019. **9**(1): p. 15421.
696 78. Takashio, S., et al., *Significance of low plasma levels of brain-derived neurotrophic*
697 *factor in patients with heart failure.* Am J Cardiol, 2015. **116**(2): p. 243-9.

698

699 **Figures**

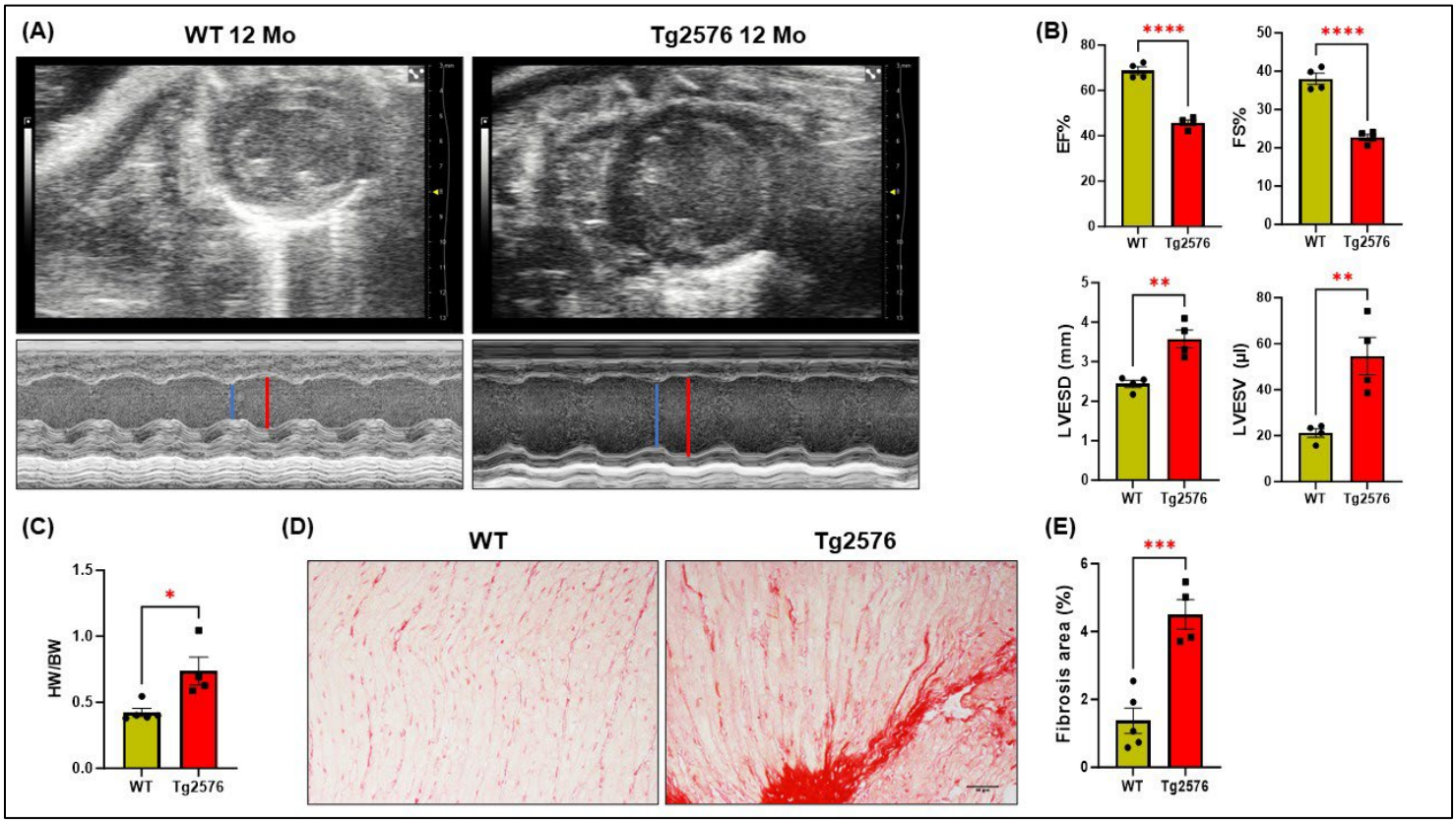

700 **Figure 1. Alzheimer's disease severely impairs cardiac tissue.** (**A**) M-mode
701 representative images of echocardiographic analysis in 12-month-old WT and Tg2576
702 mice. Red lines point to the left ventricular diameter at end-diastole while blue lines show
703 the left ventricular diameter at end-systole on M-mode images. (**B**) Left ventricle (LV)
704 systolic function is impaired in the AD model, as evidenced by a significant decline both
705 in ejection fraction (EF%) and fraction shortening percentage (FS%), accompanied by a
706 significant cardiac chamber dilation, as assessed by measuring left ventricular dimension
707 (LVESD) and left ventricular volume (LVESV) in the Tg2576 group, compared to age-
708 matched WT mice (12-month-old). (**C**) The heart weight/body weight ratio shows a
709 significant increase in Tg2576 mice compared to the WT group. (**D**-**E**) Representative
710 images (left panels) and quantitative data (right panels) showing the percentage (%) of
711 cardiac fibrosis in heart sections from WT and Tg2576 mice, assessed via PicroSirius red
712 staining (scale bar 50µm). n=4- 5 mice/group. Data are presented as a mean±SEM.

713 *P<0.05, **P<0.01, ***P<0.001, ****P<0.0001 and vs WT. Student t-tests have been
714 performed between the two groups.

715

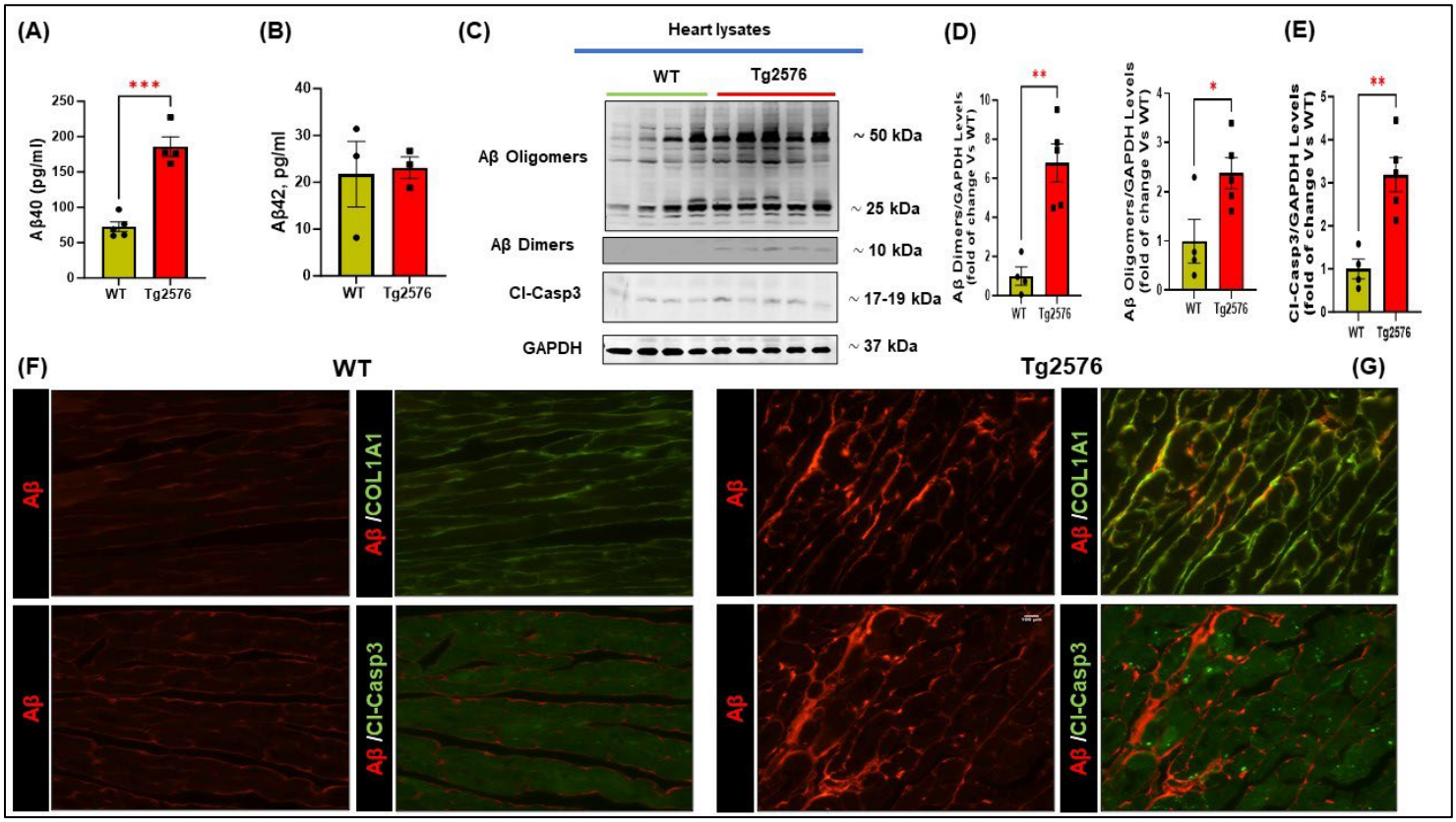

716 **Figure 2: Aβ aggregated species accumulate in the myocardial parenchyma in**
717 **association with cardiac cell apoptosis.** (**A**-**B**): Plots show Aβ40 (**A**) Aβ42 (**B**) levels
718 (pg/mL), assessed by ELISA assay in heart lysates from 12 months old WT and Tg2576
719 mice. (**C**-**E**): Representative immunoblots (left panels) and densitometric analysis (right
720 panels) showing levels of Aβ dimers, oligomers (**D**) and Cleaved-Caspase3 (Cl-Casp3,
721 **E**) in total heart lysates of 12-month-old WT and Tg2576 mice. GAPDH levels are used
722 as a loading control. (**F**-**G**): Representative digital images (top panels, scale bar 100µm)
723 showing collagen type I fibers (COL1A1, in green) and Aβ aggregates (in red) and,
724 representative digital images (bottom panels; scale bar 100µm) showing Cleaved-
725 Caspase3 (Cl-Casp3, in green) and Aβ aggregates (in red) in cardiac sections from WT
726 (left panels) and Tg2576 (right panels) mice. n=3- 5 mice/group. Data are presented as a

727 mean±SEM. *P<0.05, **P<0.01, ***P<0.001 and vs WT. Student t-tests have been
728 performed between the 2 groups.

729

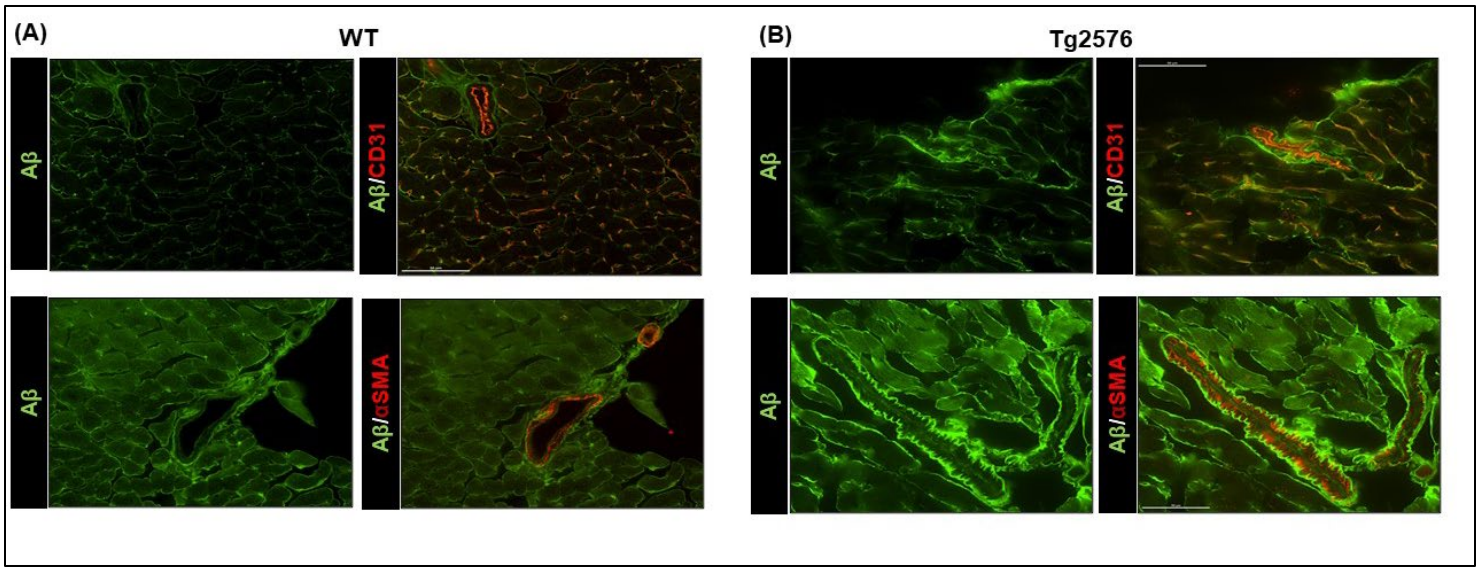

730 **Figure 3: Aβ aggregates surround cardiac vessels and infiltrate the vascular basal**
731 **lamina.** Top panels: Representative digital images (scale bar 50μm) showing endothelial
732 cells (stained with CD31, in orange) and Aβ (in green). Bottom panels: representative
733 digital images (scale bar 50μm) showing smooth muscle cells by α-Smooth muscle alpha-
734 actin staining (αSMA, in red) and Aβ (in green) in cardiac sections from WT and Tg2576
735 mice. n=3- 4 mice/group. WT mice are represented in the left panels and Tg2576 mice in
736 the right panels.

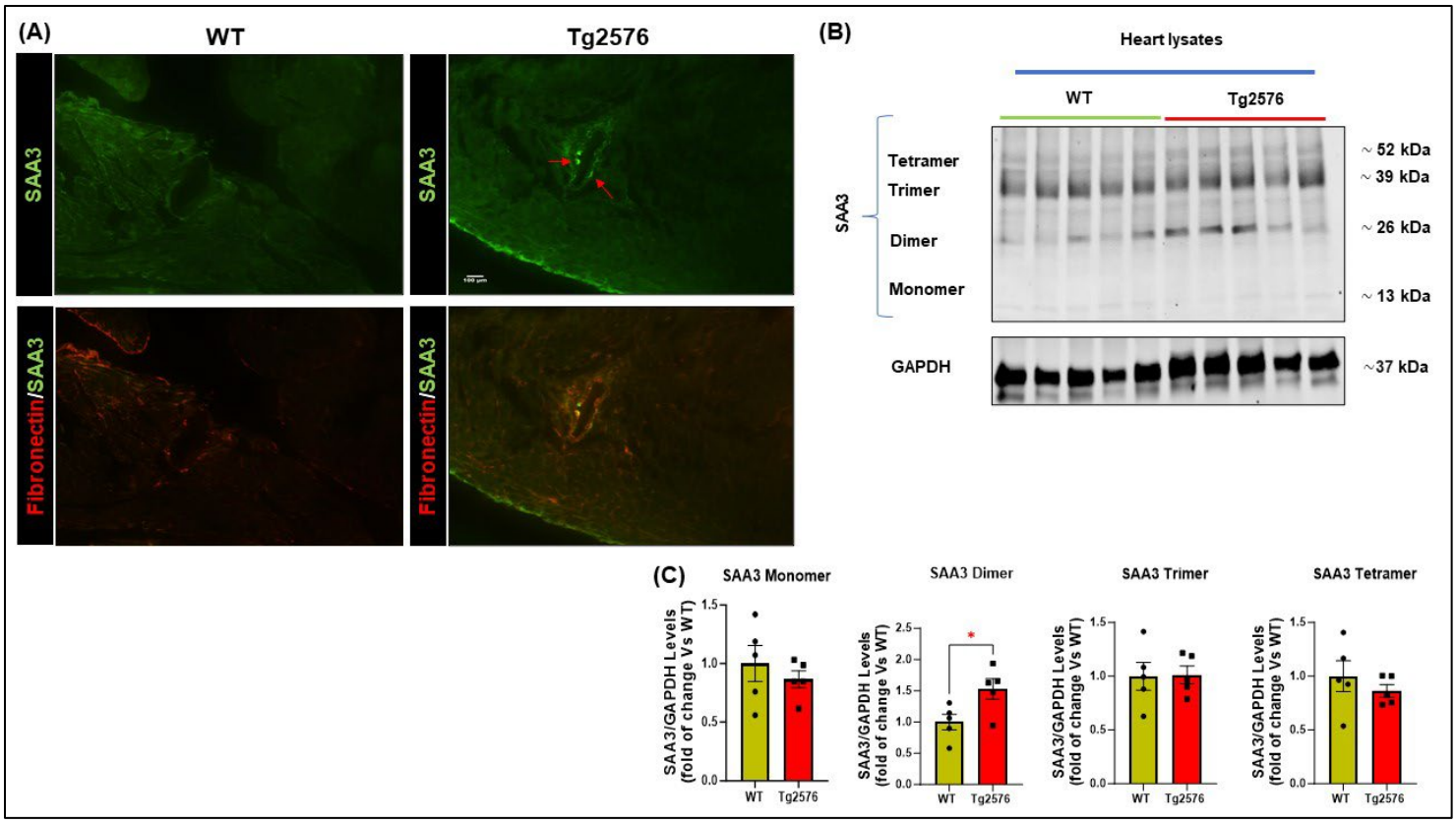

Figure 4: Serum amyloid A3 (SAA3) perivascular deposition in the heart of Tg2576 mice. (**A**): Representative images of 12-month-old WT and Tg2576 cardiac sections stained with serum amyloid A3 (SAA3, in green) and fibronectin fibers (in red, scale bar 100µm). (**B-C**): representative immunoblots (top panels) and densitometric quantitative analysis (bottom panels) showing the levels of different aggregates of SAA3 in total cardiac lysates from WT and Tg2576 mice. GAPDH levels were used as a loading control. n= 5 mice/group. Data are presented as a mean±SEM. *P<0.05 and vs WT. Student t-tests have been performed between the 2 groups.

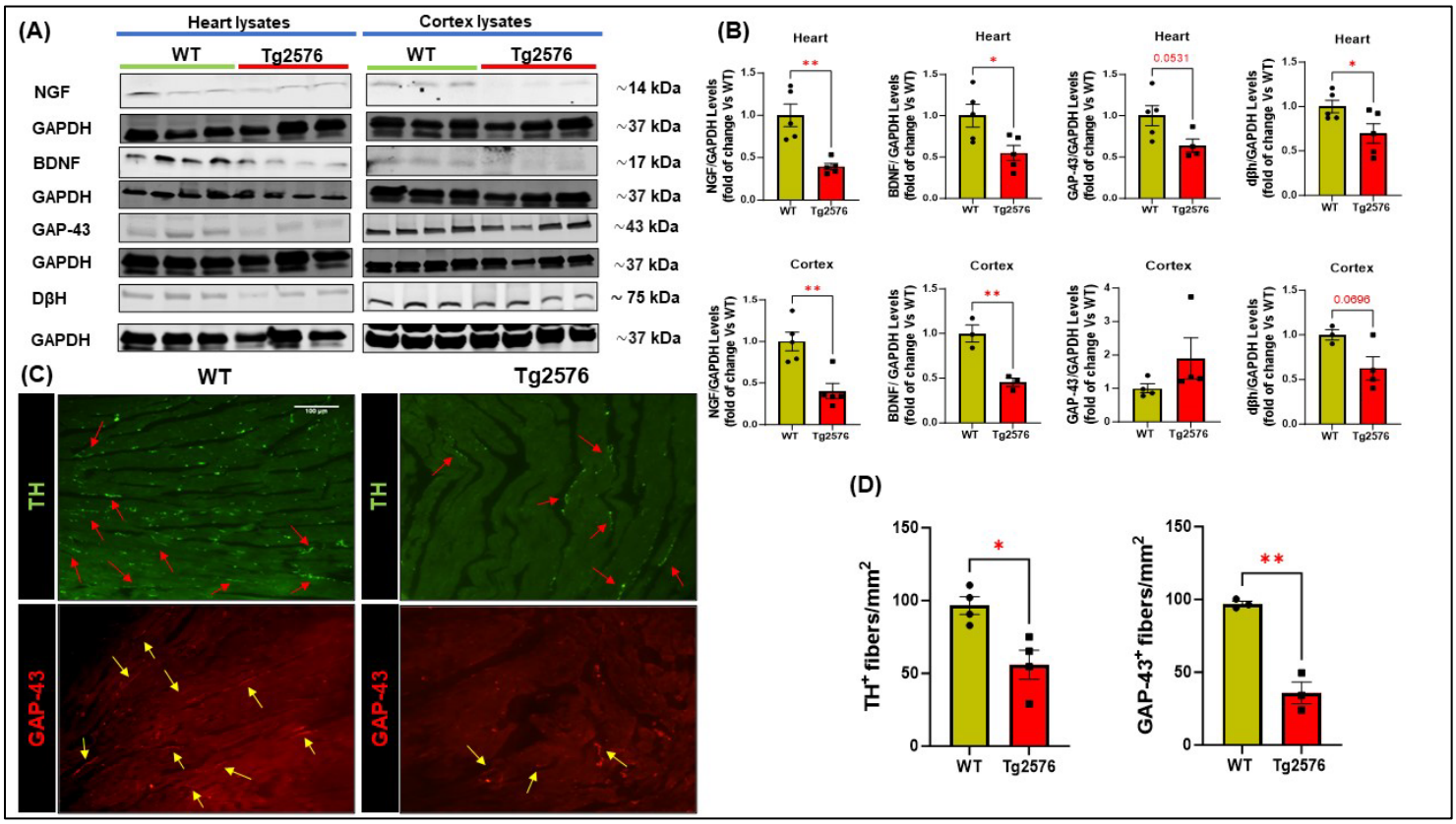

Figure 5: The neuro-signaling pathway is compromised in brain and heart of Tg2576 AD mice. (**A-B**): Representative immunoblots (**A**) and densitometric quantitative analysis (**B**) showing levels of NGF, BDNF, GAP-43, and DβH, in total cardiac (top panels) and cerebral cortex (bottom panels) lysates from WT and Tg2576 mice. (**C-D**): digital images (C, scale bar 100µm) and quantifications (D) showing cardiac adrenergic nerve fibers, labeled with anti-tyrosine-hydroxylase (TH, in green), and cardiac regenerating nerve endings, labeled with anti-neuronal regeneration marker (GAP-43, in red) in heart sections from WT and Tg2576 mice. n=3- 5 mice/group. Data are presented as a mean±SEM. *P<0.05, **P<0.01 and vs WT. Student t-tests have been performed between the 2 groups.

764

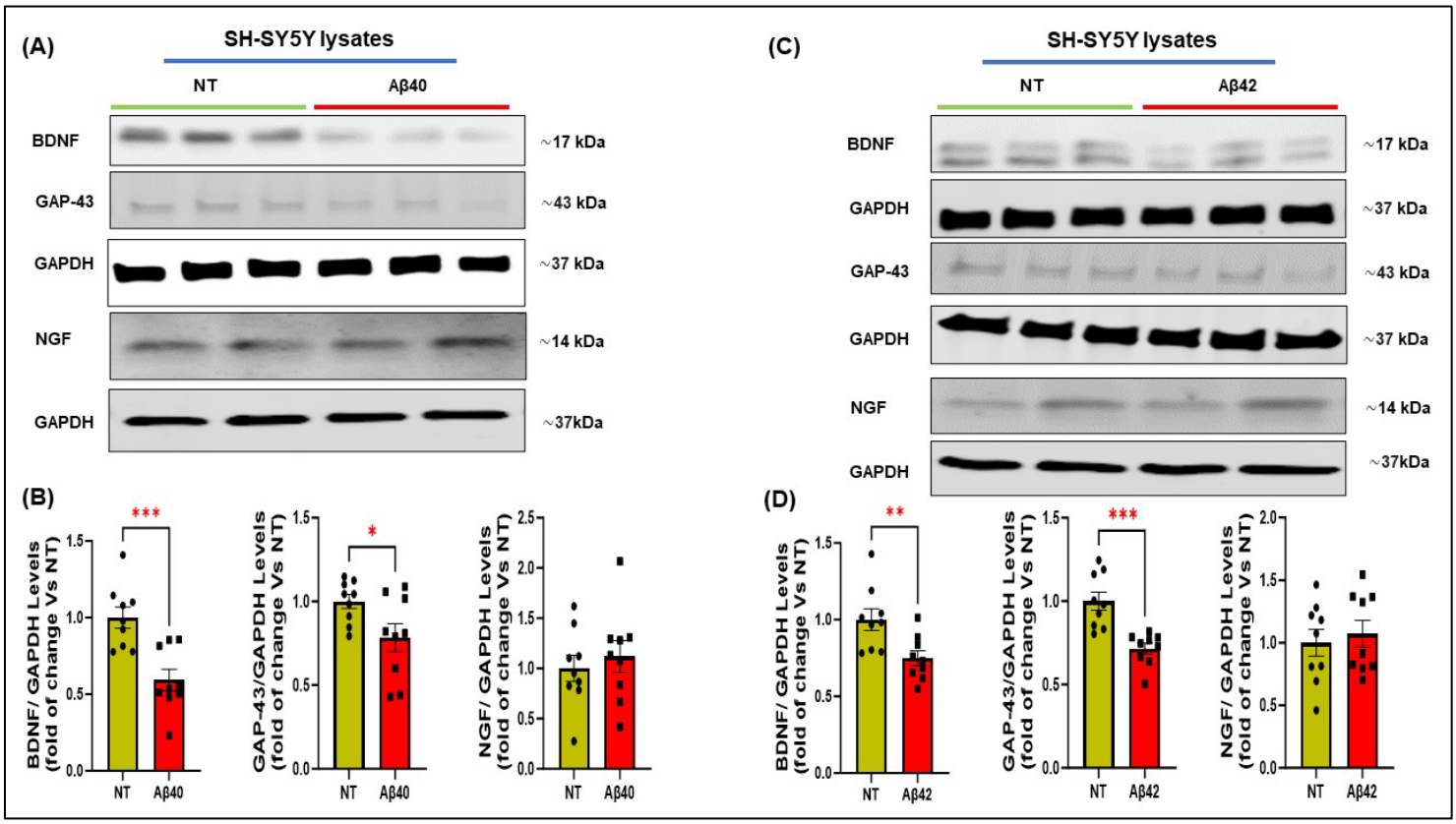

765 **Figure 6: Effects of human Aβ40 or Aβ42 oligomers on the expression of**
766 **neurotrophic factors and neuronal regeneration markers in SH-SY5Y cells**.
767 Representative immunoblots (**A** and **C**) and densitometric quantitative analysis (**B** and **D**)
768 showing protein levels of BDNF, NGF, and GAP-43 (**B**-**D**) in total protein lysates from
769 human neuroblastoma cells (SH-SY5Y) stimulated with human Aβ40 (left) or Aβ42 (right)
770 oligomers for 16 h. GAPDH levels were used as a loading control. n=9 biological
771 replicates. Data are presented as a mean±SEM. *P<0.05, **P<0.01, ***P<0.001 and vs
772 WT. Student t-tests have been performed between the 2 groups. (NT= Not Treated).

773

774

775

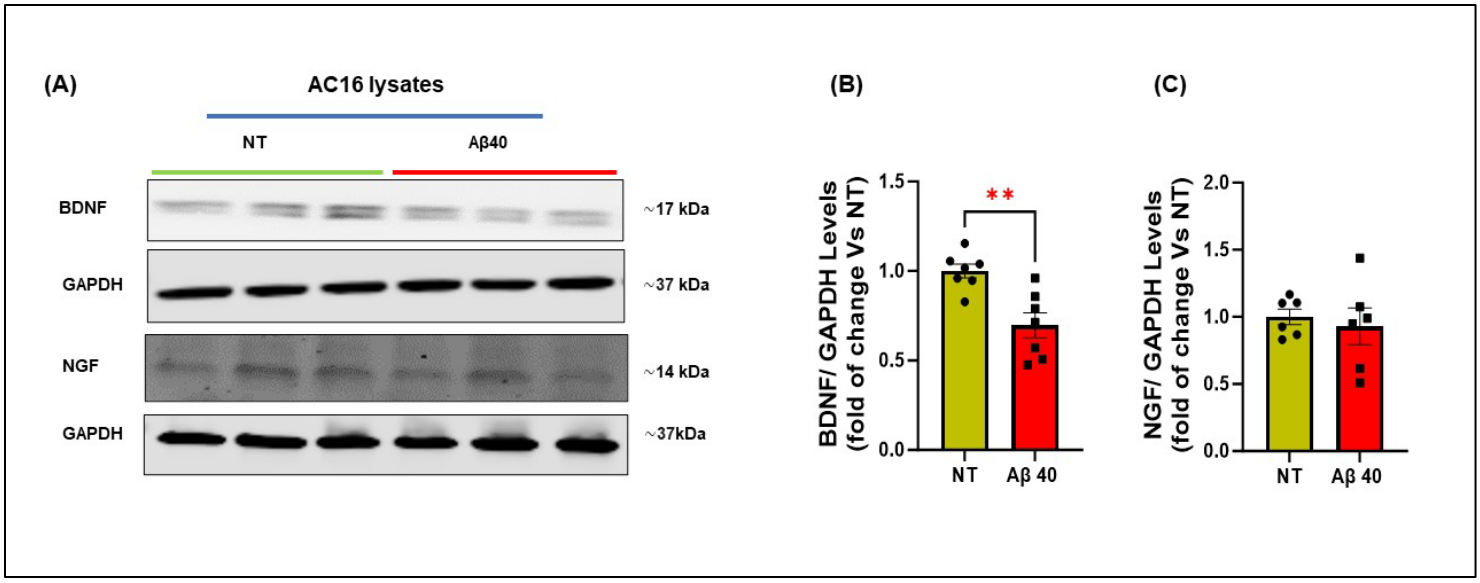

Figure 7: Effects of human Aβ40 oligomers on the expression of neurotrophic factors in AC16 Human Cardiomyocytes. (**A**-**C**): Representative immunoblots (**A**) and densitometric quantitative analysis (**B**-**C**) showing protein levels of BDNF (**B**), and NGF (**C**) in total protein lysates from human cardiomyocytes (AC16) stimulated with human Aβ-40 oligomers for 16 h. GAPDH levels were used as a loading control. n= 6-7 biological replicates. Data are presented as a mean±SEM. **P<0.01 and vs WT. Student t-tests have been performed between the groups. (NT= Not Treated).

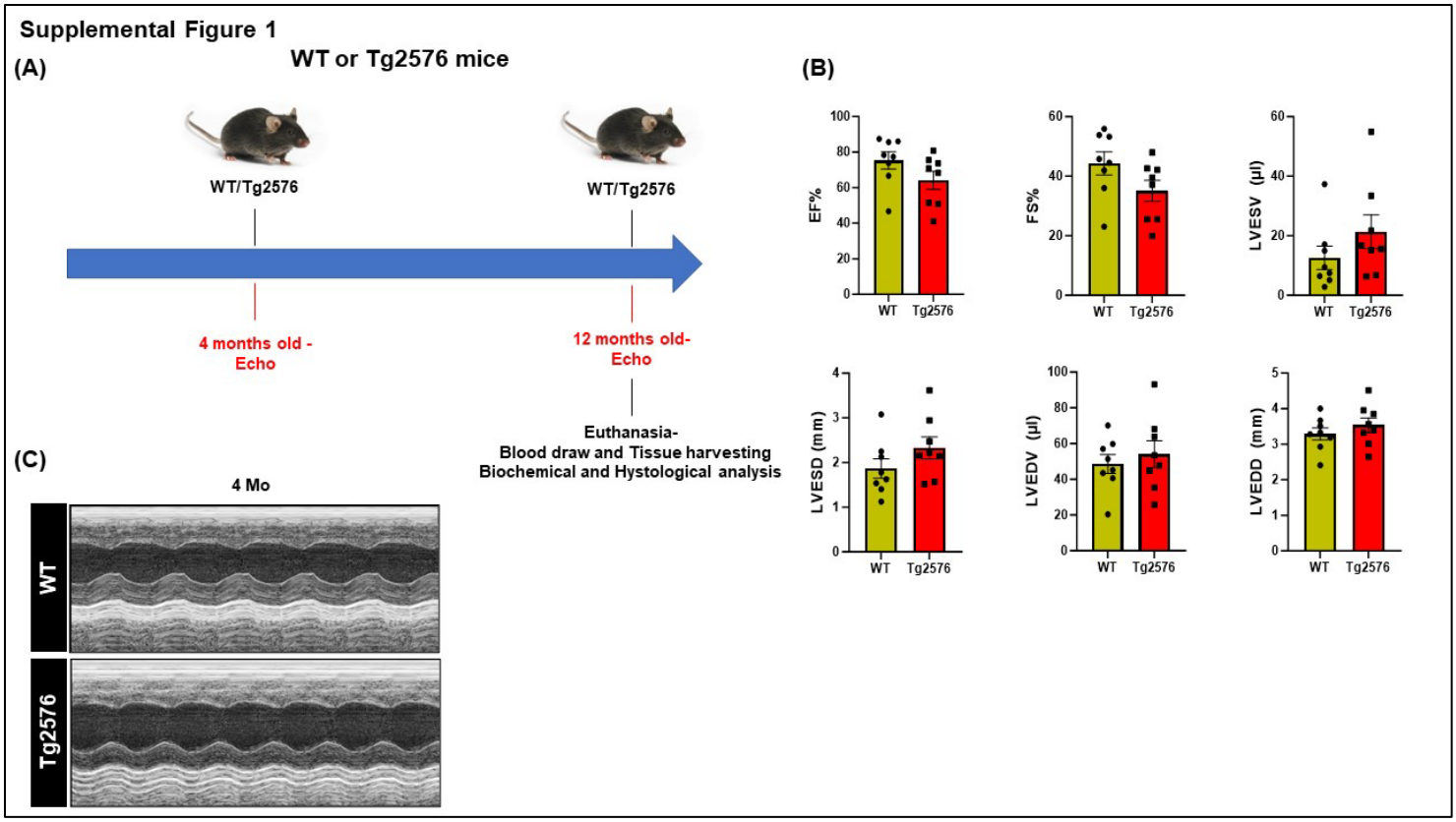

Supplemental Figure 1: Alzheimer's disease does not affect cardiac function in young Tg2576 mice. (**A**) The overall design of the 12-month study. (**B**) ejection fraction (EF%) and fractional shortening (FS%) percentage, left ventricular end-systolic and diastolic diameters (LVESD, LVEDD), and left ventricular end-systolic and diastolic volumes (LVESV, LVEDV) of Tg2576 mice and WT littermates age-matched (4-months-old). Data are presented as a mean±SEM. n= 8 mice/group. Student t-tests have been performed between the groups. (**C**) Representative M-mode echocardiography images of WT and Tg2576 mice show no difference between the two experimental groups.

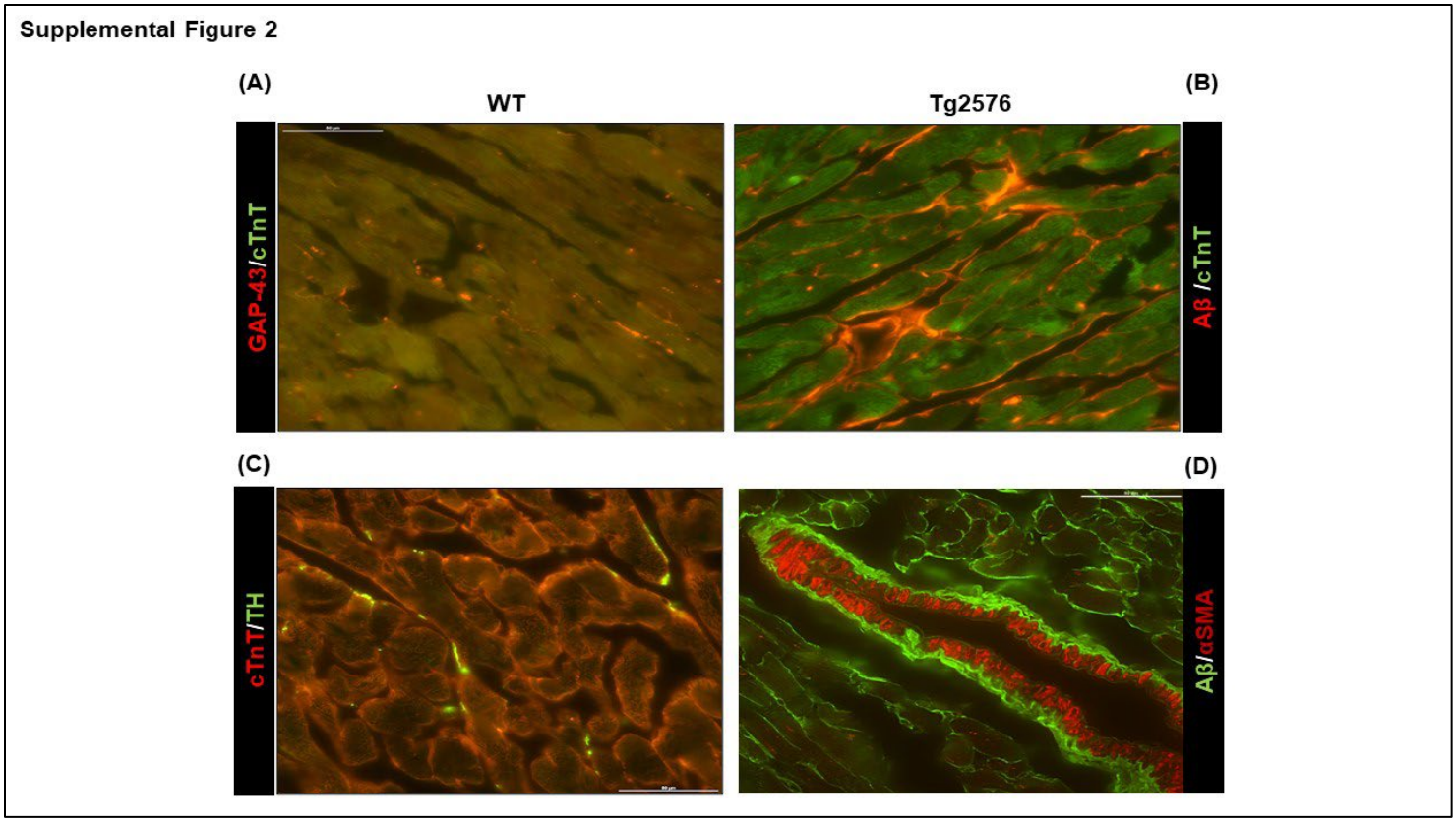

806 **Supplemental Figure 2:** Representative digital images (scale bar 50μm) of the cardiac
807 sections from WT and Tg2576 mice stained with (**A**) anti-neuronal regeneration marker
808 (GAP-43, in red) and cardiac Troponin T (cTnT, in green). (**B**) Aβ aggregates (in red) and
809 cardiac Troponin T (cTnT, in green). (**C**) anti-tyrosine-hydroxylase (TH, in green) and
810 cardiac Troponin T (cTnT, in red). (**D**) Aβ aggregates (in green) and α-Smooth muscle
811 actin (α-SMA, in red).